The International Journal of Advanced Manufacturing Technology (2019) 102:2231–2243
https://doi.org/10.1007/s00170-019-03371-4

ORIGINAL ARTICLE

A predictive model of subsurface damage and material removal volume for grinding of brittle materials considering single grit micro-geometry

Wenyang Liu[1] · Liang Zhang[1] · Qihong Fang[1] · Jianbin Chen[2]

Received: 5 September 2018 / Accepted: 20 January 2019 / Published online: 29 January 2019

Abstract

It has been proven that micro-geometry of abrasive grits can influence the maximum cutting depth, thereby strongly affecting the material removal mechanism in grinding of brittle materials. The influence of grit micro-geometry on subsurface integrity, however, is not yet fully understood. In this paper, we aim to understand how grit micro-geometry affects subsurface damage and the material removal volume. An analytical model that takes into account grit micro-geometry and the intrinsic material removal mechanism is developed for predictions of material removal volume and subsurface damage. Results show that increasing the apex angle or grit tip radius tend to deteriorate subsurface integrity by extending the depth of subsurface damage. Moreover, it is found that the grit tip radius strongly affects the ductile-to-brittle transition in one grit pass along the contact trajectory. If ductile-to-brittle transition occurs in a grit pass with the brittle mode dominated, the predictive model indicates that the material removal volume decreases with an increasing apex angle or edge radius of abrasives. On the other hand, non-monotonic dependence of material removal volume on grit micro-geometry turns up for ductile-material removal in grinding of brittle materials. The predictive model is validated qualitatively and quantitatively, demonstrating good agreement with earlier reports. The proposed predictive model enables making proper choice of highly engineered abrasives in grinding of brittle materials.

Keywords Micro-grinding · Subsurface damage · Brittle material removal · Micro-geometry · Ductile regime machining

1 Introduction

The demand for brittle materials has been continuously growing in optical industries because of their attractive properties including bubble-free characteristics, stable optical qualities, low amount of inclusions, high electrical isolation, high resistance to corrosion, wear, chemicals, and heat [1]. Grinding is one of the most effective ways to machine brittle materials [2, 3]. Brittle materials, however, suffer from poor machinability due to high hardness, high brittleness, and low fracture toughness. Therefore, it is of great importance to study the mechanism of material removal and machining induced part integrity degradation in grinding of brittle materials.

Material removal mechanisms generally can be categorized into two types: brittle fracture and ductile deformation. In grinding of brittle materials, brittle fracture often occurs, and materials are removed through the propagation and intersection of cracks. It was first found by Giovanola and Finnie [4] that the ductile mode of material removal can be achieved in machining of certain types glasses. Since then, ductile material removal in grinding of brittle materials has been investigated and has been actively studied. It was reported by many researchers that the scale of grinding operations affects the material removal mode. Bifano

✉ Wenyang Liu
liuwenyang@hnu.edu.cn

Qihong Fang
fangqh1327@hnu.edu.cn

[1] State Key Laboratory of Advanced Design and Manufacturing for Vehicle Body, Hunan University, Changsha, Hunan Province 410082, People's Republic of China

[2] Piezoelectric Device Laboratory, School of Mechanical Engineering and Mechanics, Ningbo University, Ningbo, Zhejiang Province 315211, People's Republic of China

et al. [5] investigated analytically and experimentally the infeed rates necessary for ductile-regime grinding of brittle materials and showed that all brittle materials can undergo plastic flow if the depth of machining is small enough. Liu et al. [6] proved that ductile chip formation can be achieved if the undeformed chip thickness is small enough and the undeformed chip thickness is smaller than the tool cutting edge radius. Arif et al. [7] proposed a model to predict critical undeformed chip thickness for ductile-to-brittle transition. Zhu et al. [8] demonstrated that the maximum undeformed chip thickness is a governing factor for ductile-regime grinding. Chen et al. [9] used single grit experiment tests to investigate the brittle-to-ductile transition in micro-grinding of single crystal silicon and developed a model to describe the energy interaction. A review of ductile regime machining was given by Neo et al. [10].

The mechanism of material removal plays a decisive role in surface and subsurface damage in grinding of brittle materials. Two principal crack systems, i.e., lateral cracks and median cracks, are involved in formation of damage [11]. Lateral cracks are responsible for material removal, and median cracks are responsible for strength degradation [12]. Many efforts have been conducted to study subsurface damage developed during grinding of brittle materials theoretically. A model for subsurface damage estimation from abrasive sizes was developed by Lambropoulos [13]. Jing et al. [14] proposed an analytical model for investigating deformation and machining-induced damage associated with brittle solids. Gu et al. [15] developed a model describing the correlation between scratch hardness and the depth of subsurface cracks for optical glass BK7. Chen et al. [16] suggested that the depth of median crack can be correlated with the plastic deformation zone based on the work of Jing et al. [14]. Taking into account elastic stress field to the median crack propagation in grinding of brittle materials, Li et al. [17] suggested a theoretical model describing the relationship between surface roughness and subsurface damage. Wang et al. [18] discussed the relationship between subsurface damage and grinding parameters considering kinematic characteristics of the micro-grinding processes. Quan et al. [19] studied the depth of subsurface damage in micro-grinding of brittle materials with consideration of abrasive grit rotations, and their results indicate that both the median and lateral cracks incline gradually as the angle of rotation increases. Malkin and Guo [20] derived the maximum penetration for idealized grinding wheels with triangular abrasive grits equally spaced around the wheel periphery. Song and Yin investigated [21] the quantitative effect of diamond bur grit sizes on subsurface damage, and their results indicate that smaller grit sizes tend to reduce subsurface damage. Axinte et al. [22] studied the influence of single grit micro-geometry on grinding behavior of ductile and brittle materials and enabled choosing proper grit shapes for machining brittle materials.

Besides theoretical studies, experimental studies have provided much information on subsurface damage. Grinding mechanisms for ceramics were studied using a technological basis for cost-effective machining by Malkin and Hwang [23]. Li et al. [24] evaluated the subsurface damage of BK7 glasses and found that the theoretical ratio of subsurface damage to surface roughness is directly proportional to loads of abrasive grains and hardness of optical materials. Xu et al. [25] investigated the maximum cutting depth generated after sawing granite over a wide range of operating conditions, and the experiments indicate that the maximum cutting depth is related to the active grit geometry and machined parameters. Pei et al. [26] investigated the effects of grinding parameters such as feedrate and wheel rotational speed on the depth of subsurface crack by a set of factorial design experiments. Randi et al. [27] established a method for estimating the depth of subsurface damage by correlating surface microroughness measurements to the depth of subsurface damage in grinding of single crystalline optical materials. The depth and distribution of subsurface damage induced by rotary ultrasonic machining and conventional grinding processes were studied by Lv et al. [28]. It was found that the surface qualities can be improved by increasing cutting velocities or decreasing workpiece feed velocities. Ohta [29] examined the subsurface damage and proposed using the small-tool polishing method and the slanted-polishing method to reduce the depth of finishing removal. Simulations and numerical experiments were used as effective tools to investigate the material removal mechanism and the effect of grinding parameters on ground surface quality using finite element simulations [30–32].

Not only machining difficulty, but also machining efficiency involved with grinding of brittle materials is an impediment to application of advanced materials. Major factors that influence machining rate are static force, vibration amplitude, rotating speed, grid size, and grit number. Hu et al. [33] presented a predictive model of the material removal rate and shedded light into the material removal mechanism. Schmitz and Ziegert [34] presented an empirical equation of material removal ratio related to the axial depth of cut, radial depth of cut, and linear feed rate in milling processes. Ramesh et al. [35] reported experimental evaluation of ultra-high speed advanced ceramic grinding and showed that the material removal rate increases with increasing wheel speed. An expression of material removal rate considering the specific energy consumption was derived by Peng and Xu [36]. Bastawros et al. [37] used the finite element method to analyze the material removal rate in chemical-mechanical planarization process. Wang et al. [38] noted that the material removal volume increases with increasing grinding depths or apex angles of abrasive grits.

Though considerable efforts have been spent to study subsurface damage and material removal rate in grinding of brittle materials, no detailed study has been reported on effects of grit micro-geometry on subsurface damage and material removal volume for machining of brittle materials that account for both brittle and ductile material material mechanisms. In this paper, we aim to analytically understand the influences of grit shapes on subsurface damage and material removal volume including sharp abrasive grits with various half apex angles and round grits with different edge radii. The remaining of this paper is arranged as follows. Section 2 presents a formula for predicting subsurface damage and material removal volume. Section 3 discusses the influence of grit micro-geometry parameters on subsurface damage. Section 4 summarizes concluding remarks.

2 Model formulation

2.1 Single-grit micro-grinding model

Figure 1 shows a schematic plot of undeformed chip with a length of l generated by a single grit in micro-grinding processes. h_i is the instantaneous cutting depth of the abrasive grit increasing from 0 to the maximum undeformed chipthickness h_m. b_i is the effective grinding width of a grit.

To study the influence of grit micro-geometry, both sharp and round abrasive grits are considered in the present study. A grit with perfectly sharp edge can be described by the half apex angle α as shown in Fig. 1a. For round abrasive grits, the tip radius R is considered as shown in Fig. 1b. The effects of grit size and geometric effects on subsurface damage and material removal processes are intrinsically complicated, it is therefore worth making a few assumptions as

i Abrasive grits are considered as rigid cones;
ii Elastic recovery is ignored as the cutting depth is much larger than the elastic recovery depth;
iii Effects of tool vibration are ignored, and the grinding process is assumed continuous; and
iv The instantaneous effective rake angle of a grit is considered to be the same as the half apex angle.

The analogy for peripheral surface grinding is illustrated in Fig. 2. The chip outflows along the instantaneous rake angle in micro-grinding is shown in Fig. 2a. Grinding related parameters are illustrated in Fig. 2b, in which v_s is the grinding wheel speed, v_w is the workpiece speed, a_p is the grinding depth, h_m is the maximum cutting depth, and d_w is the grinding wheel diameter. The effective wheel diameter de is expressed as [20]

$$d_e = d_w(1 + v_w/v_s)^2. \tag{1}$$

The maximum angular rotation angle θ_m is given as [39]

$$\theta_m = \arcsin(2\sqrt{a_p/d_e}). \tag{2}$$

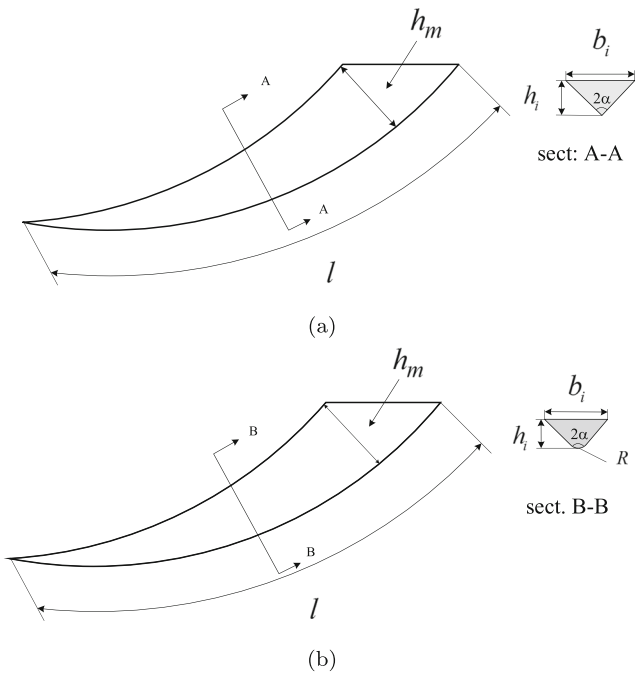

Fig. 1 Undeformed chip with **a** triangular cross-section with sharp tip and **b** triangular cross-section with a round tip

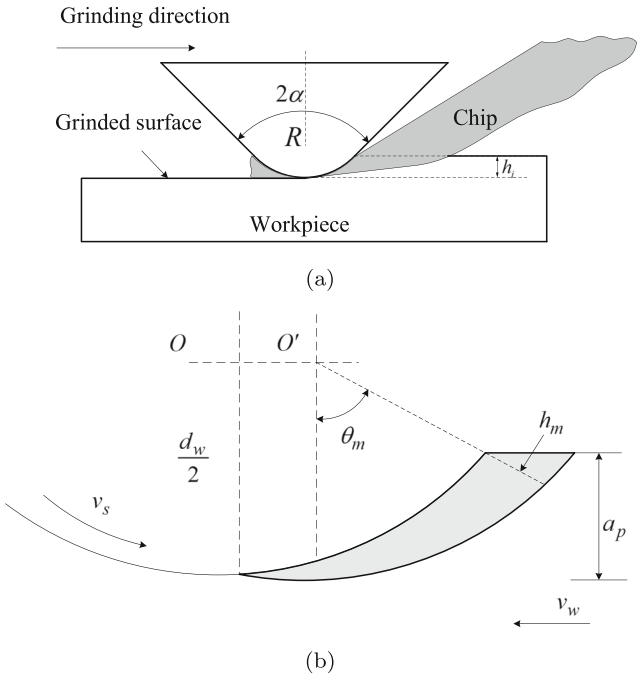

Fig. 2 **a** Geometry schematic of peripheral surface grinding and **b** parameters associated with micro-grinding by a single-grit

The instantaneous cutting depth h_i is given as [39]

$$h_i = \frac{h_m}{2}\sqrt{\frac{d_e}{a_p}}\theta_i. \tag{3}$$

To derive the maximum cutting depth h_m of round-tip grits, we follow the procedure in [20]. The spacing L between successive cutting points is [20]

$$L = \frac{1}{C\bar{b}}, \tag{4}$$

where C is the number of active grits per unit area, and $\bar{b}$ is the average effective grinding width of a grid depending on the grit geometry and the average cutting depth $\bar{h}$ as

$$\bar{b} = 2\left(\bar{h} + \frac{R}{\sin\alpha} - R\right)\tan\alpha \tag{5}$$

Since h_m is very small for micro-grinding, $\bar{h}$ can be approximately taken as half of the maximum cutting depth

$$\bar{h} = \frac{h_m}{2}. \tag{6}$$

Hence, the spacing between successive cutting points can be calculated as

$$L = \frac{\cos\alpha}{C(h_m\sin\alpha + 2R - 2R\sin\alpha)}. \tag{7}$$

By considering the single grit grinding process, the maximum cutting depth (undeformed chip thickness) h_m depends on the undeformed chip length and grinding parameters as [20]

$$h_m = 2L\frac{v_w}{v_s}\sqrt{\frac{a_p}{d_e}}. \tag{8}$$

Substituting Eq. 7 into Eq. 8 and solving for h_m, the maximum cutting depth is found to be

$$h_m = \frac{1}{Cv_s}\left(CRv_s - CRv_s\csc\alpha \pm\sqrt{(-CRv_s + CRv_s\csc\alpha)^2 + 2C\sqrt{\frac{a_p}{d_e}}v_s v_w\cot\alpha}\right) \tag{9}$$

Because the half apex angle is in the range of $0 < \alpha < \pi/2$, h_m must be non-negative

$$h_m = \frac{1}{Cv_s}\left(CRv_s - CRv_s\csc\alpha + \sqrt{(-CRv_s + CRv_s\csc\alpha)^2 + 4C\sqrt{\frac{a_p}{d_e}}v_s v_w\cot\alpha}\right) \tag{10}$$

Setting the tip radius to 0 μm, Eq. 10 reduces to

$$h_m = \sqrt{\frac{2v_w\cot\alpha}{Cv_s}}\sqrt{\frac{a_p}{d_e}}, \tag{11}$$

which is equivalent to the derivation of maximum undeformed chip thickness for sharp grits in [20]. Thereby, the correctness of Eq. 10 is verified.

2.2 Volume of material removed by ductile and brittle modes

In micro grinding, the volume of material removal is affected by grit micro-geometry. Depending on the maximum cutting depth, two scenarios need to be considered.

1. *The maximum cutting depth h_m is smaller than the edge radius.* Material is removed in the ductile mode along the grit pass [6], and the contact trajectory length, denoted by l_d in Fig. 3, is

$$l_d = l, \tag{12}$$

where $l = \sqrt{a_p d_e}$ is the full contact length of a grit. The cross-sectional area A^d depends on the value of h_m as

$$A^d = \begin{cases} A_1^d & \text{for } h_m \leqslant R(1-\sin\alpha) \\ A_2^d & \text{for } R(1-\sin\alpha) < h_m \leqslant R \end{cases} \tag{13}$$

$$A_1^d = \frac{1}{2}(\pi - 2\alpha)R^2 - R^2\sin\alpha\cos\alpha \tag{14}$$

$$A_2^d = \left(R\cos\alpha + \frac{R}{\cos\alpha} - R\tan\alpha + h_m\tan\alpha\right) \times(h_m - R + R\sin\alpha) + \frac{1}{2}(\pi - 2\alpha)R^2 - R^2\sin\alpha\cos\alpha \tag{15}$$

The material removal volume per grit per pass is

$$V^d = \begin{cases} V_1^d & \text{for } h_m \leqslant R(1-\sin\alpha) \\ V_2^d & \text{for } R(1-\sin\alpha) < h_m \leqslant R \end{cases} \tag{16}$$

$$V_1^d = \int_0^l A_1^d\left(1 - \frac{z}{l}\right)^2 dz \tag{17}$$

$$V_2^d = \int_0^{l_1} A_1^d\left(1 - \frac{z}{l}\right)^2 dz + \int_0^{l-l_1} A_2^d\left(1 - \frac{z}{l}\right)^2 dz \tag{18}$$

where

$$l_1 = \frac{R(1-\sin\alpha)l_d}{h_m}. \tag{19}$$

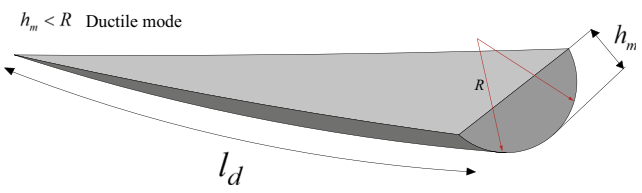

Fig. 3 The geometry of material removal volume by plastic flow

After substituting the expression of A^d, V^d can be evaluated

$$V_1^d = \frac{1}{6}(\pi - 2\alpha)R^2 l_d - \frac{1}{3}R^2 l_d \sin\alpha\cos\alpha. \tag{20}$$

$$V_2^d = \frac{1}{6}(\pi - 2\alpha)R^2 l_d - \frac{1}{3}R^2 l_d \sin\alpha\cos\alpha + \frac{{l_d}^3 - {l_1}^3}{3{l_d}^2}\left(R\cos\alpha + \frac{R}{\cos\alpha} - R\tan\alpha + h_m\tan\alpha\right) \times (h_m - R + R\sin\alpha). \tag{21}$$

2. *The maximum cutting depth h_m is larger than the edge radius.* The ductile material removal mode first takes places since the grit cutting depth h_i is still smaller than the edge radius. The length denoted by l_d can be determined as

$$l_d = \frac{R}{h_m}l. \tag{22}$$

Once the grit cutting depth is greater than the edge radius, the material removal mode switches to brittle mode as shown in Fig. 4 with the contract trajectory length denoted by l_b . Therefore, we can write

$$l_b = l - l_d. \tag{23}$$

In brittle mode, material is removed by crack propagation that originates from lateral cracks beneath the plastically deformed region [40]. A schematic plot of subsurface damage consisting of lateral and median cracks is shown in Fig. 5. By assuming that the lateral crack length c_l varies proportionally, the cross-section area can be approximated by

$$A^b = \frac{1}{2}\pi\left[c_l^{\max}\left(1 - \frac{z}{l}\right)\right]^2, \tag{24}$$

where z is the distance to the maximum lateral crack length $c_l^{\max}$. The material removal volume in brittle mode is

$$V^b = \int_0^{l-l_d} A^b dz = \frac{l^3 - l_d^3}{6l^2}\pi(c_l^{\max})^2. \tag{25}$$

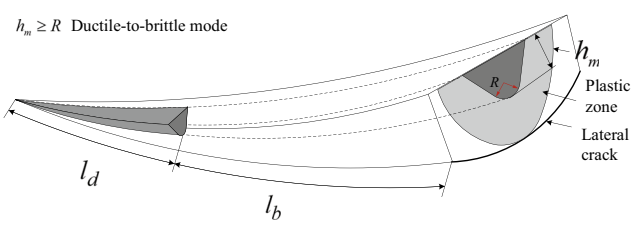

Fig. 4 The geometry of material removal volume by plastic flow and brittle fracture

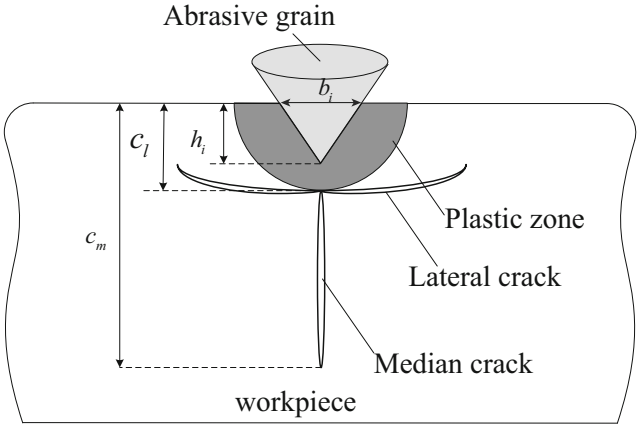

Fig. 5 Schematic plot of cracks induced by scratching brittle materials

Therefore, the total volume of material removed along the grit contact trajectory is

$$V = V^d + V^b = \frac{1}{6}(\pi - 2\alpha)R^2 l_1 - \frac{1}{3}R^2 l_1 \sin\alpha\cos\alpha + \frac{l^3 - l_d^3}{6l^2}\pi(c_l^{\max})^2. \tag{26}$$

The evaluation of $c_l^{\max}$ will be given in the following section.

2.3 Depth of median cracks and subsurface damage

The analogy for peripheral surface grinding is represented in Fig. 6. In this schematic model, the distance between the tip of grinding grit and the final grinding surface y_i can be obtained as [20]

$$y_i = \frac{1}{4}d_e\theta_i^2, \tag{27}$$

where θ_i is the abrasive grit rotation in micro-grinding.

When the maximum cutting depth h_m is smaller than the edge radius, material is removed in the ductile mode [6], leaving behind a crack-free machined surface [5]. In

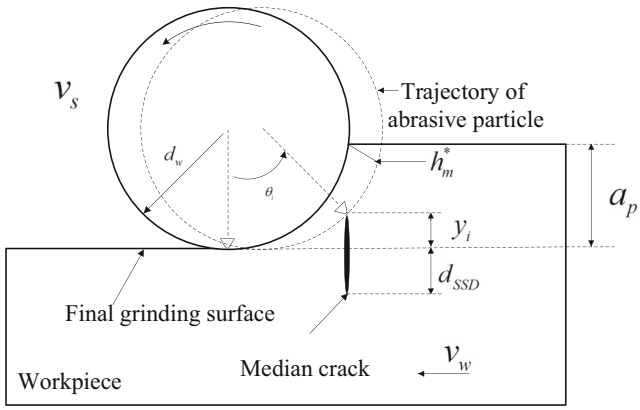

Fig. 6 Schematic plot of horizontal surface grinding

Table 1 Material properties of optical glass BK7 [15]

Properties	Value
Young's modulus E(GPa)	82
Poisson's ratio ν	0.203
Vickers hardness H_s (GPa)	7.7
Fracture toughness K_c (MPam$^{1/2}$)	0.82
Active grit density C (grit/mm^2)	3.2

contrast, when the maximum cutting depth h_m is greater than the edge radius, ductile-to-brittle transition takes place as the grit cutting depth increases from 0 to h_m as shown in Fig. 4. Hence, there exists a critical rotation angle θ_c where mode switching occurs

$$\theta_c = \frac{2R}{h_m}\sqrt{\frac{a_p}{d_e}}. \tag{28}$$

It has been found that two lateral cracks and one median crack usually appear in grinding of brittle materials [11] as shown in Fig. 5. The depths of median and lateral crack, denoted by c_m and c_l respectively, are given as [14–16]

$$c_m = 0.206\left(\frac{E}{H_s}\right)^{1/3}(\cos\alpha)^{4/9}\left(\frac{P}{K_c}\right)^{2/3}, \tag{29}$$

$$c_l = \left[\frac{3(1-2\nu)}{5-4\nu} + \frac{2\sqrt{3}}{\pi(5-4\nu)}\frac{E}{\sigma_y}\cot\alpha\right]^{1/2} h_i\tan\alpha, \tag{30}$$

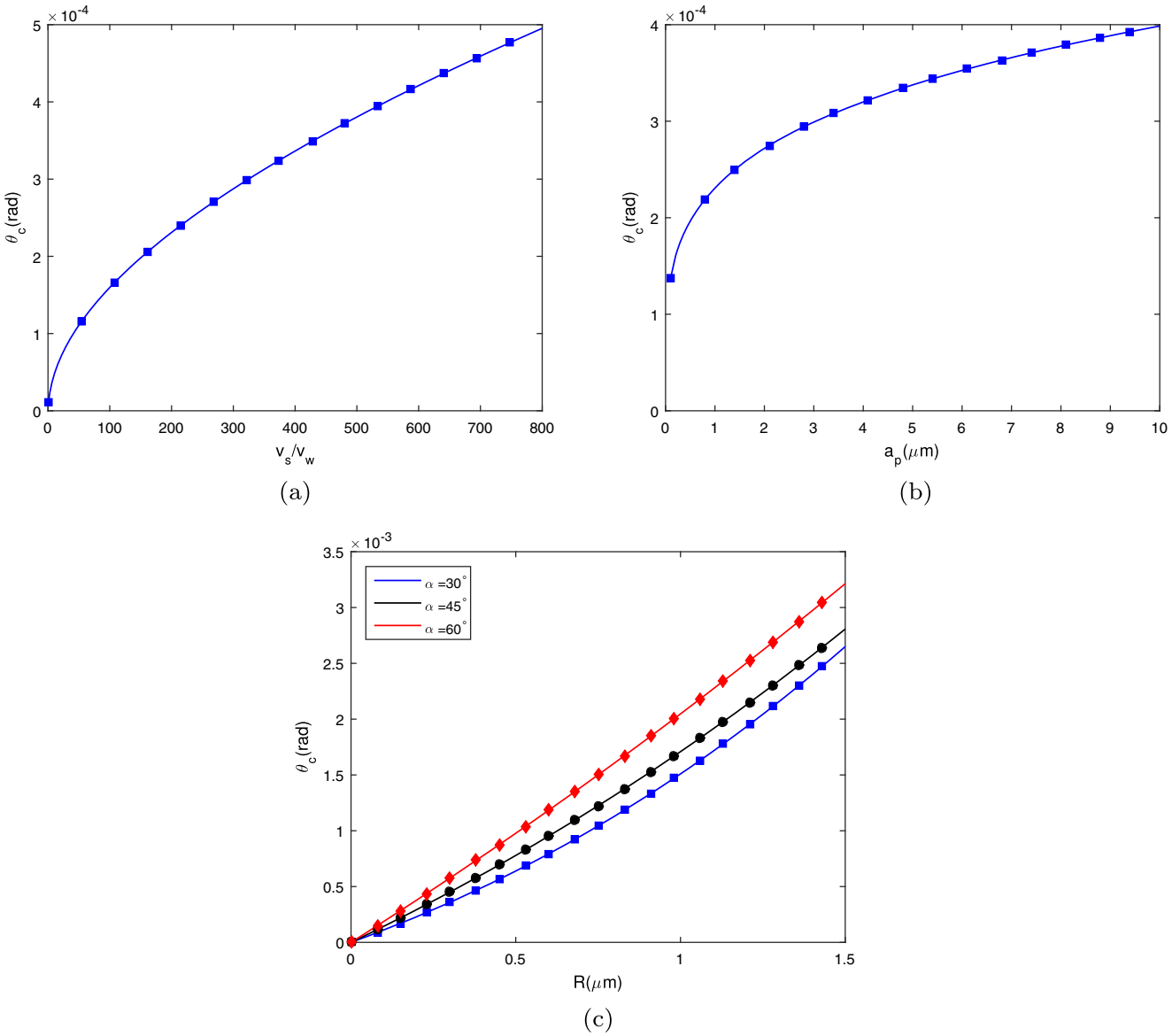

Fig. 7 The critical angle θ_c versus **a** the ratio v_s/v_w, **b** the grinding depth a_p, and **c** the grit tip radius

where P is the normal force, H_s is the scratch hardness of workpiece materials, K_c is fracture toughness, β is the elastic recovery coefficient, E is Young's modulus, ν is the ratio of Poisson, and σ_y is the yield stress. The maximum lateral crack length $c_l^{\max}$ can be determined by substituting h_i with h_m in Eq. 29.

For round-tip grits, the projection of contact area in the normal direction is

$$A_N = \pi(h_i - R + R/\sin\alpha)^2 \tan^2\alpha. \tag{31}$$

Scratch hardness is defined as [41]

$$H_s = \frac{P}{A_N}. \tag{32}$$

By substitutive Eqs. 31 and 32 into Eq. 29, the depth of median crack considering grit micro-geometry is obtained as

$$c_m = 0.442\frac{(E H_s)^{1/3}}{K_c^{2/3}}(\tan\alpha)^{4/3}(\cos\alpha)^{4/9}(h_i + \frac{R}{\sin\alpha} - R)^{4/3}. \tag{33}$$

The depth of subsurface damage generated by grinding of brittle materials depends on the depth of median cracks, grit cutting depth, and grit rotation as

$$d_{SSD} = c_m - h_i\cos\theta_i - y_i. \tag{34}$$

After substituting Eq. 29 into Eq. 34, the final equation of d_{SSD} can be obtained.

3 Results and discussions

In the following sections, the proposed predictive model is used to investigate the grit size effect on the volume of material removal and subsurface damage. Various apex angles and grit tip radii are studied. Material properties of the workpiece used in case studies are summarized in Table 1.

3.1 Effect of grit micro-geometry on material removal volume

The material removal volume depends on the material removal mechanisms. Under the condition of $h_m \leqslant R$, material removal is accomplished via severe plastic deformations. For $h_m > R$, ductile-to-brittle transition occurs in a grit pass because the instantaneous engaged depth h_i is continuously increasing. Hence, it is meaningful to evaluate the critical angle θ_c at which the mode switching occurs. As a case study, the edge radius is set to $R = 0.2\mu$ m to ensure that the condition $h_m > R$ is satisfied, the half apex angle is $\alpha = 30°$, and $d_w = 400$ mm. The maximum cutting depth is $h_m = 1.28$ μm by evaluating Eq. 8. It is found that the critical angle θ_c increases with increasing v_s/v_w ratio or the grinding depth as shown in Fig. 7a. By setting the ratio v_s/v_w to a constant, the influence of a_p on the critical angle θ_c is shown in Fig. 7b. Note that v_s/v_w is set to 200 for case studying, and changing v_s/v_w does not affect the general trend. Additionally, the influence of edge radius on the critical angle θ_c is demonstrated in Fig. 7c for various apex angles. Increasing the edge radius or apex angle is beneficial in term of achieving larger θ_c, meaning a larger portion of material is removed in the ductile mode.

Figure 8a plots the relationship between the maximum cutting depth h_m against the half apex angle α. In general, the maximum cutting depth decreases as the half apex angle increases. It is also evident that the maximum cutting depth

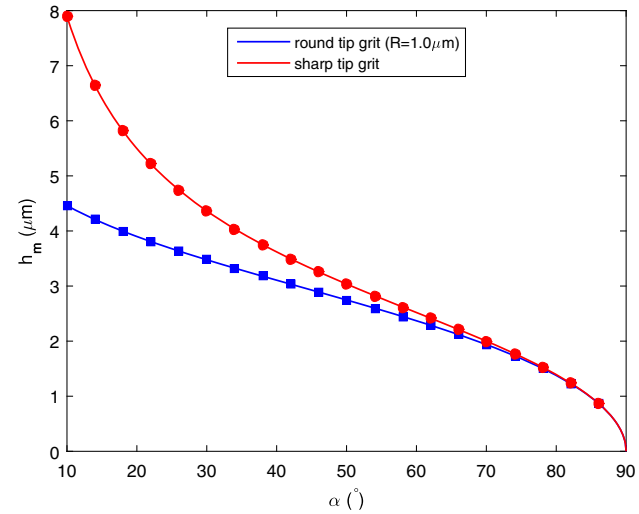

(a)

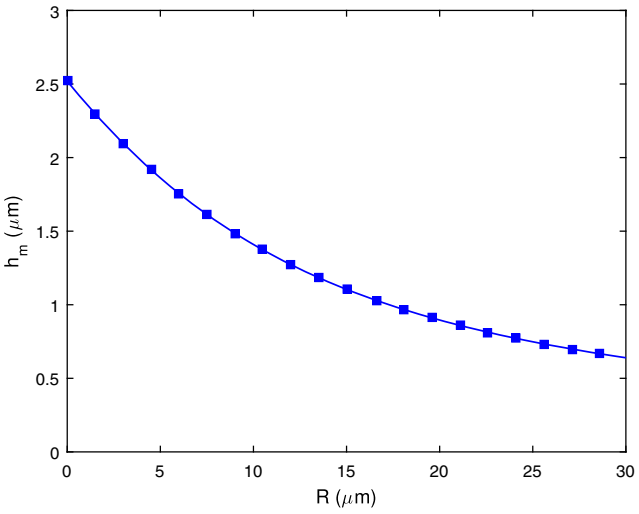

(b)

Fig. 8 The maximum cutting depth h_m versus **a** the half apex angle of the abrasive grit α and **b** the grit tip radius R

h_m generated by round grits is lower than that generated by sharp grits. It is worth noting that the difference in h_m between sharp grits and round grits reduces as the half apex angle increases. With a half apex angle of 70°, the difference in h_m due to grit tip geometry is only around 3.5%. Hence, the effect of tip radius is negligible for large half apex angles. Figure 8b shows the effect of grit tip radius on the maximum cutting depth with the half apex angle set to 60°. h_m decreases as the tip radius increases for round abrasives. Our observations regarding the grit size effect on the maximum cutting depth is consistent with the study by William et al. [41].

Figure 9 shows the relationship between the maximum cutting depth and grit tip radius for various half apex angles. The general trend is that the maximum cutting depth decreases as the grit tip radius increases. In addition, the half apex angle affects the maximum cutting depth. When the tip radius is small, sharper grits result in greater cutting depths. For instance, considering perfectly sharp grits ($R = 0\ \mu$m), h_m is approximately 4.2 μm for $\alpha = 30°$, greater than $h_m = 2.5\ \mu$m for $\alpha = 60°$ by 68%. More importantly, it is found that smaller half apex angles lead to greater cutting depths for small grit tip radii ($R < 3\ \mu$m approximately). This trend, however, is reversed for grits with a large edge radius. In Fig. 9, addition lines representing $h_m = R$ and $h_m = R(1 - \sin\alpha)$ are plotted. As mentioned in Section 2, materials are removed in the ductile mode if $h_m < R$. In contrast, if $h_m \geqslant R$, material is removed in the ductile mode first, and the mode switching from the ductile mode to the brittle mode occurs once the rotation angle reaches θ_c. The conditions of $h_m = R$ are 2.20 μm, 2.45 μm, 2.55 μm for half apex angles of 30°, 45°, 60°, respectively. Given the condition of $h_m \geqslant R$, the material removal volume in a grit pass can be calculated by evaluating Eq. 26.

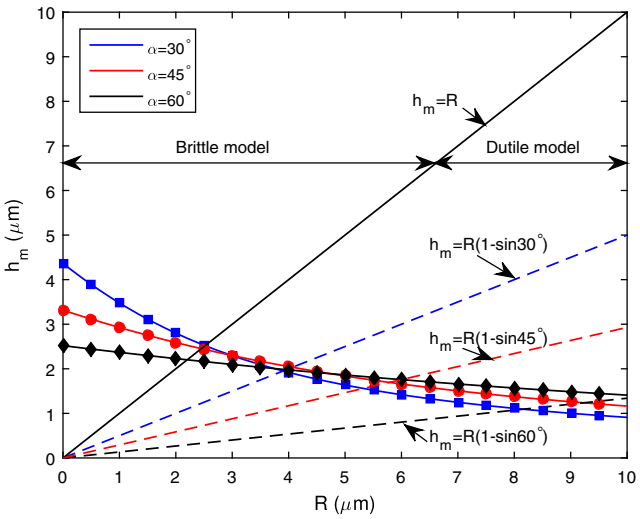

Fig. 9 The maximum cutting depth h_m versus tip radius R for different apex angles

The effect of tip radius on the material removal volume under the condition of $h_m > R$ is demonstrated in Fig. 10a. It is observed that the volume decreases as the radius increases, and larger material removal volumes are obtained for smaller half apex angles. On the other hand, given the condition $h_m < R$, two scenarios exist, i.e., $h_m < R(1 - \sin\alpha)$ and $R(1 - \sin\alpha) \leqslant h_m < R$ as described by Eq. 16. The effect of increasing R on the material removal volume is non-monotonic as shown in Fig. 10b. For $\alpha = 30°$, the condition of $h_m = R(1 - \sin\alpha)$ is reached when $R = 3.9\ \mu$m; for $\alpha = 45°$, the condition of $h_m = R(1 - \sin\alpha)$ is reached when $R = 5.79\ \mu$m; for $\alpha = 60°$, the condition of $h_m = R(1 - \sin\alpha)$ is reached when $R = 10.34\ \mu$m by referring to Fig. 9.

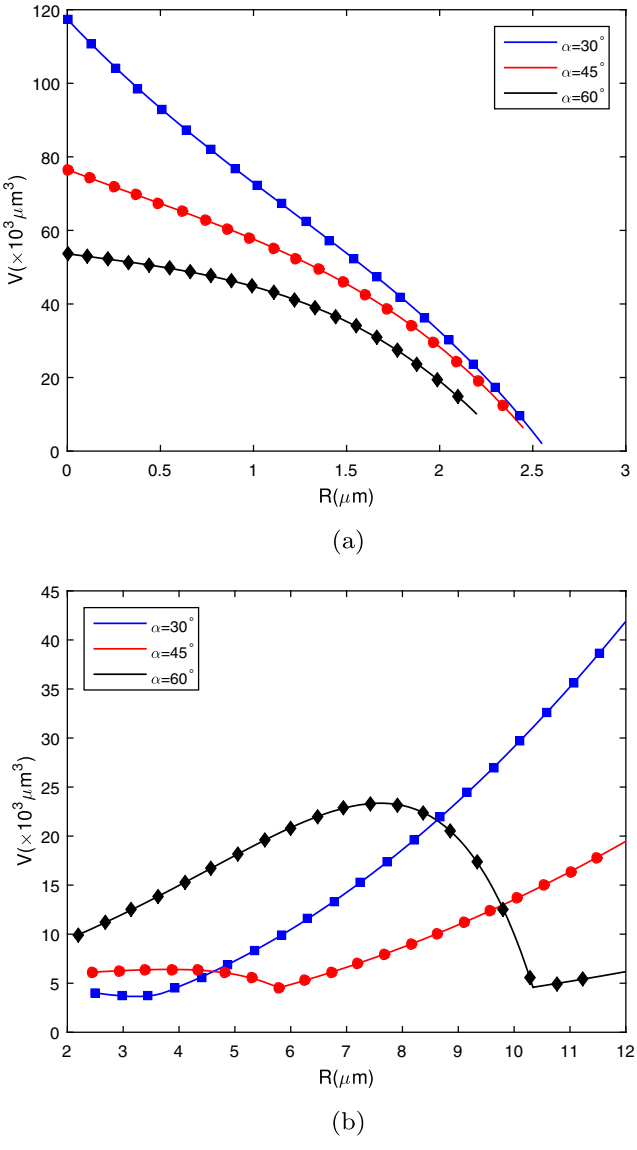

Fig. 10 The influence of tip radius R on the material removal volume in **a** ductile-to-brittle mode under the condition of $h_m > R$ and **b** ductile mode

3.2 Effect of grit micro-geometry on subsurface damage

The evolution of median crack depth as a grit rotates is shown in Fig. 11. For sharp abrasive grits (i.e., grit tip radius $R = 0$ μm), median cracks show up as soon as the grit comes into contact with the workpiece. To investigate grit size effect on subsurface damage, the tip radius is set to 0.5 μm, and the half apex angle is set to 30°. The calculated maximum cutting depth is $h_m = 3.89$ μm. Since the maximum cutting depth is greater than the edge radius, the material is first removed in the ductile mode without causing damage and then removed in the brittle mode that induces subsurface damage in the workpiece. As indicated by Eq. 28, the ductile–brittle transition takes place as the critical angle of rotation θ_c is reached. The calculated critical angle of rotation θ_c for ductile-to-brittle transition is 0.0009 rad as indicated by the dashed line in Fig. 11a. It is observed that the depth of median crack increases as grit the rotates, consistent with the simulations conducted by Wang et al. [18]. Another observation from Fig. 11a is that although c_m is small initially for the sharp grit, the value of c_m increases faster compared to that associated with round grits. Figure 11b shows the relationship between the median crack depth and rotation angle for various half apex angles. It is observed that larger half apex angles lead to deeper median crack depths. In addition, it is found that increasing grit tip radius tends to increase θ_c, meaning that more material is removed in the ductile mode for grits with larger tip radii. The critical rotation angles of ductile-to-brittle transition θ_c are 0.0009 rad, 0.0011 rad, and 0.0014 rad for half apex angles of 30°, 45°, and 60°, respectively.

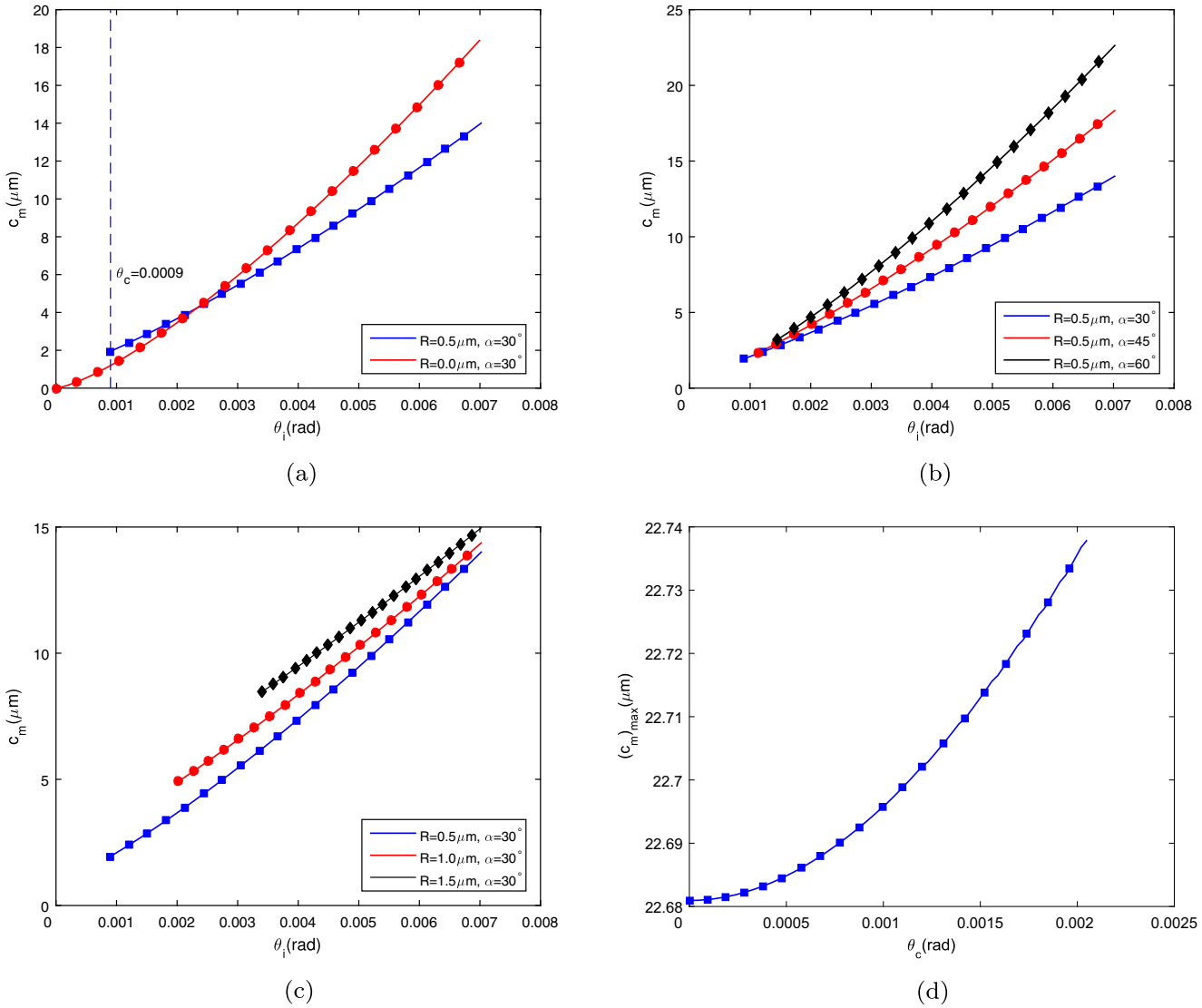

Fig. 11 Influence of **a** sharp versus round grit tip, **b** abrasive grit half apex angle α, **c** grit edge radii R, and **d** different the critical angle θ_c on the depth of the median crack c_m

The effect of grit tip radius on the median crack depth is shown in Fig.11c. It is evident that larger grit tip radii cause deeper median cracks. Figure 11d demonstrates that the maximum depth of median crack increases as the critical angles θ_c increases.

Figure 12a plots the predicted depth of subsurface damage for varying half apex angles. The trend is similar to that of c_m. Subsurface damage increases as grit rotates, and larger half apex angles lead to severer subsurface damage. The effect of grit tip radius on the depth of the subsurface damage is shown in Fig. 12b. Figure 12c shows that the maximum subsurface damage increases with the critical angle, indicating that there is a trade-off to be made: to achieve fine grinding quality, larger θ_c is desired in order to have larger volume of materials removed in the ductile mode in a grit pass; the downside of larger θ_c, however, is that larger maximum median cracks are induced, deteriorating part integrity.

3.3 Validation of the predictive model

Grinding experiments were conducted to study subsurface damage. The material selected for this experiment is the optical glass BK7. The dimension of the workpiece is 60 mm × 40 mm × 20 mm. Experiments were carried out on the high-speed grinder MKL7132X8/17. The wheel has a diameter of 400 mm and a width of 15 mm. Typical subsurface damage after grinding tests is shown in Fig. 13. Lateral cracks are readily observed, rationalizing the use of maximum lateral crack length in the predictive model of material removal volume in the brittle mode.

To investigate the influence of grit micro-geometry on material removal volume in a grit pass and induced subsurface damage, it is desired to use engineered grinding tools with controlled abrasive shapes. Cheng et al. [9] reported an experimental study on brittle-ductile transition using single grit scratching tests. In single scratching passes with decreasing cutting depth as shown in Fig. 14, mode transitions are observed, bolstering the theoretical analysis of ductile-to-brittle mode transition presented in Section 2. Predictions of the effect of apex angle on subsurface damage shown in Figs. 11b and 12a agree with the experimental observation that larger angles cause severer fracture in workpiece. Additionally, the experimental observation that increasing grinding speed tend to extend the ductile-mode removal length in a grit pass can also be explained by our analytical model. By substituting Eq. 10 into Eq. 22, it can be show that the ductile-mode removal length is proportional to $\sqrt{V_s V_w}$.

To qualitatively validate the analytical model, the predicted subsurface damage is compared against experimentally

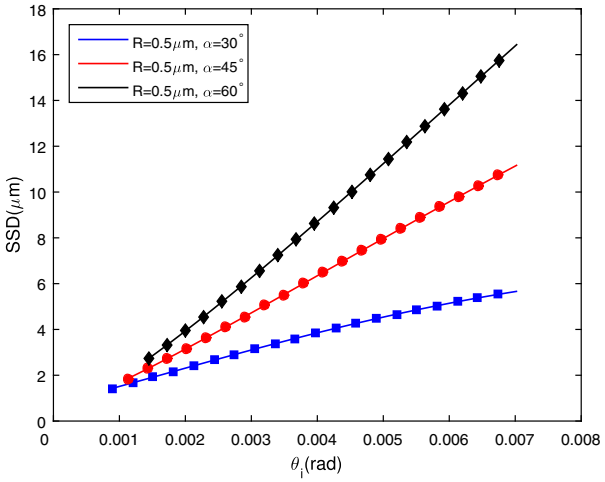

(a)

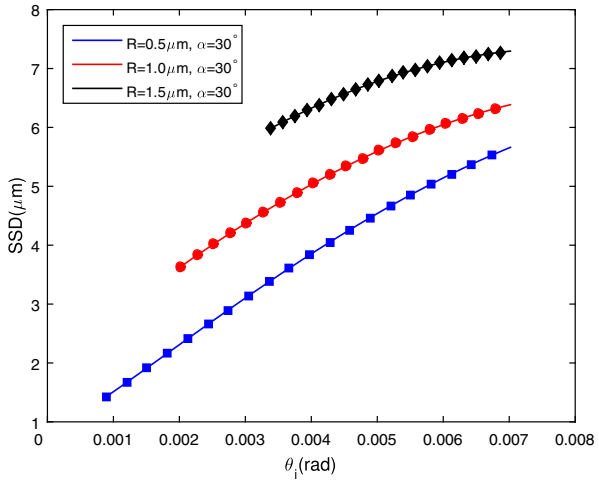

(b)

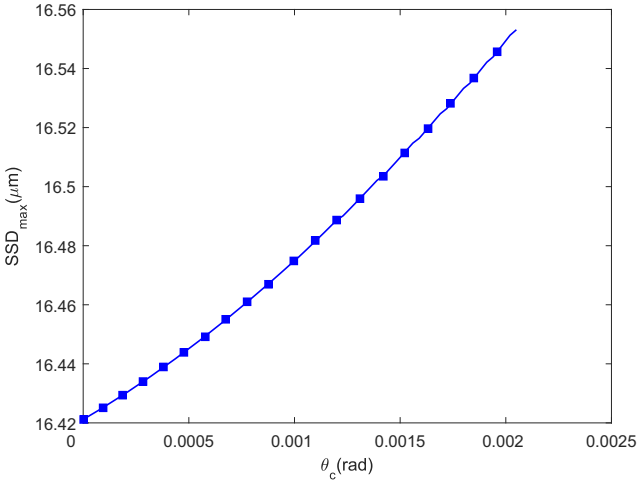

(c)

Fig. 12 The depth of the subsurface damage (SSD) versus **a** abrasive grit half apex angle α, **b** grit edge radius R, and **c** the critical angle θ_c

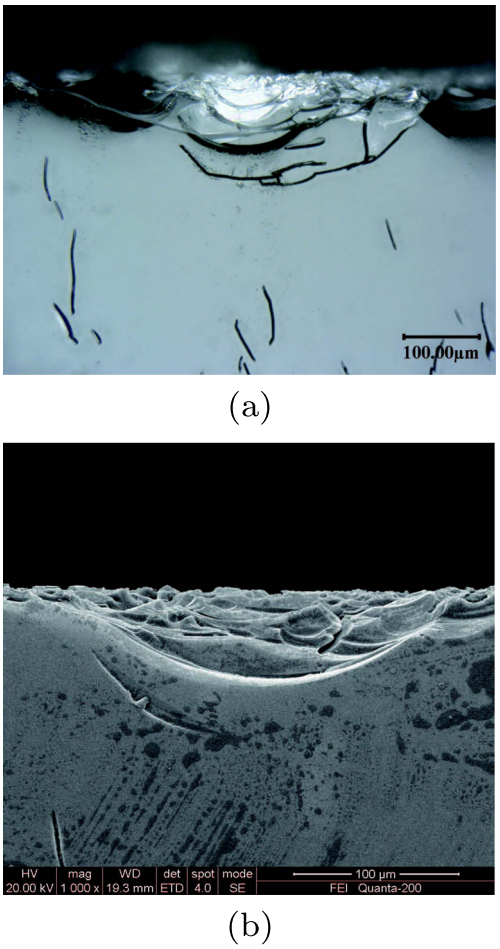

Fig. 13 Observations of typical subsurface damage by **a** optical microscopy and **b** SEM

fitted lower and upper bounds suggested by Lambropoulos [13] as $0.3L^{0.68} < \text{subsurface damage}(\mu\text{m}) < 2L^{0.85}$ in terms of the grid size L. The lower and upper bounds are valid for all optical glasses, BK7 included, and regardless of feeds and speeds [13]. In the present study, the same parameters as those in previous case studies are used, i.e., $v_s/v_w = 200$, $a_p = 5\ \mu$m, and $d_w = 400$ mm. The grit tip radius is $R = 2\ \mu$m. With $\alpha = 60°$, $h_m = 2.23\ \mu$m. Keeping constant the maximum undeformed chipthickness

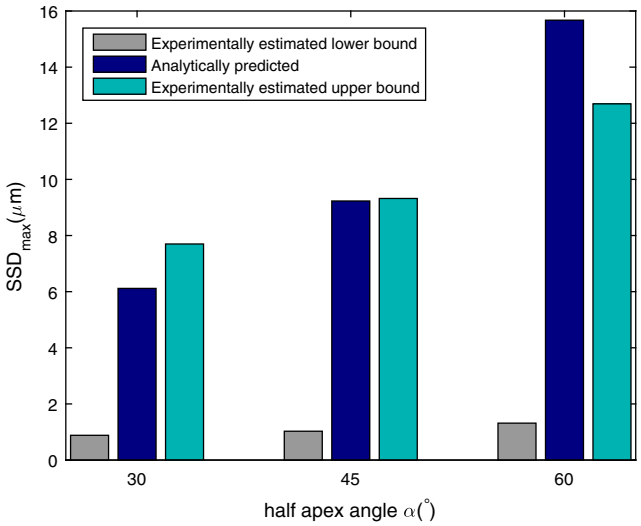

Fig. 15 Comparison of predicted maximum subsurface damage against experimentally fitted bounds [13]

h_m and varying the apex angle lead to different contact area sizes. For half apex angles of 30°, 45°, and 60°, the radii of projected contact area, illustrated in Fig. 5 as b_i, are 4.88 μm, 6.12 μm, and 8.80 μm, respectively. By setting b_i as the grid size L, the lower and upper bounds of subsurface damage can be determined. The comparison between analytical predictions and experimentally fitted bounds is shown in Fig. 15. It can be seen that analytical predictions of subsurface damage are very close to the upper bounds determined from the experiments for the half apex angle $\alpha \leqslant 45°$. On the other hand, the analytical model overpredicts the subsurface damage for $\alpha = 60°$. Note that the median crack depth c_m describe by Eq. 29 is more appropriate for sharp grits. A grit with the apex angle of $2\alpha = 120°$ is rather blunt, tending towards generating inclined double cracks rather than a single median crack [9].

Lastly, analytical predictions of subsurface damage for various apex angles are supported by the simulations conducted by Wang et al. [18]. Severer subsurface damage is observed for larger the apex angles in their simulations, and collapse phenomenon shows up in workpiece for the apex angle $2\alpha = 120°$.

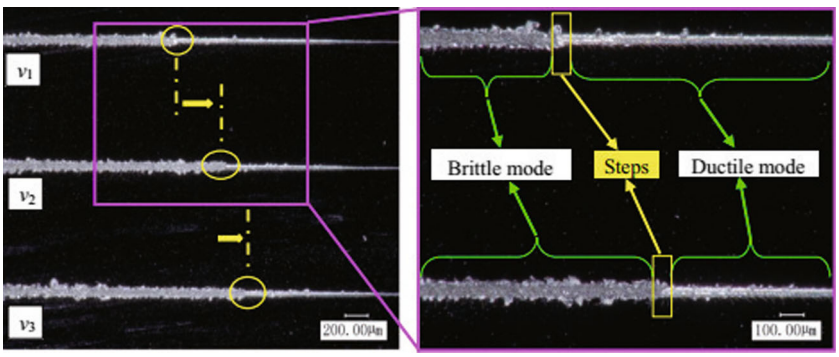

Fig. 14 Experimental observations of ductile-to-brittle transition in a single path of scratching test with decreasing cutting depth. Adapted from [9] with permission

4 Conclusions

In this paper, a predictive model of material removal volume and subsurface damage with consideration of grit micro-geometry is proposed. Depending on the size of edge radius compared to the maximum undeformed chip thickness, ductile or ductile-to-brittle material removal mechanism can be invoked. For ductile material-removal with the properties of brittle materials, no subsurface damage is induced and material is removed by forming severely sheared chips. On the other hand, brittle material-removal induces subsurface damage, the material removal volume in a grit pass needs to consider the length of lateral cracks.

The effects of the grit edge radius and the apex angle on subsurface damage and material removal volume are studied. The main conclusions are summarized as follows. The critical angle of ductile-to-brittle transition depends on grit micro-geometry and machining parameters as well. Increasing the apex angle or the edge radius tend to decrease the maximum undeformed chip thickness, a decisive factor for material removal mechanisms. Under the condition of the undeformed chip thickness larger than the edge radius, material removal volume in a single pass is dominated by brittle fracture, and the predictive model indicates that the materials removal volume decreases as the edge radius or the apex angle. On the other hand, under the condition of the undeformed chip thickness smaller than the edge radius, there is a non-monotonic dependence of material removal volume on grit micro-geometry. Lastly, the maximum subsurface damage increases with the critical angle. Larger tip radii result in a greater volume of material removed in the ductile mode. But severer subsurface damage is caused after the material removal mode is switched to the brittle mode.

Funding information This study received support from the National Natural Science Foundation of China (NNSFC) through grant no. 11572118 and no. 11702089.

References

1. Zhang C, Zhang J, Feng P (2013) Mathematical model for cutting force in rotary ultrasonic face milling of brittle materials. Int J Adv Manuf Technol 69(1):161–170
2. Jackson MJ, Robinson GM (2006) Surface grinding of space materials using specially formulated vitrified grinding wheels. J Mater Eng Perform 15(2):242–246
3. Bandyopadhyay BP (1995) The effects of grinding parameters on the strength and surface finish of two silicon nitride ceramics. J Mater Process Technol 53:533–543
4. Giovanola JH, Finnie I (1980) On the machining of glass. J Mater Sci 15(10):2508–2514
5. Bifano TG, Dow TA, Scattergood RO (1991) Ductile-regime grinding: a new technology for machining brittle materials. J Eng Ind 113(2):184–189
6. Liu Kui, Li XP, Liang SY (2007) The mechanism of ductile chip formation in cutting of brittle materials. Int J Adv Manuf Technol 33(9):875–884
7. Arif M, Zhang X, Rahman M, Kumar S (2013) A predictive model of the critical undeformed chip thickness for ductile–brittle transition in nano-machining of brittle materials. Int J Mach Tools Manuf 64:114–122
8. Zhu D, Yan S, Li B (2014) Single-grit modeling and simulation of crack initiation and propagation in sic grinding using maximum undeformed chip thickness. Comput Mater Sci 92:13–21
9. Cheng J, Wu J, Gong YD, Wen XL, Wen Q (2017) Experimental study on the single grit interaction behaviour and brittle–ductile transition of grinding with a diamond micro-grinding tool. Int J Adv Manuf Technol 91(1-4):1209–1226
10. Neo WK, Kumar AS, Rahman M (2012) A review on the current research trends in ductile regime machining. Int J Adv Manuf Technol 63(5-8):465–480
11. Maksoud TMA, Mokbel AA, Morgan JE (1999) Evaluation of surface and sub-surface cracks of ground ceramic. J Mater Process Technol 88(1):222–243
12. Agarwal S, Venkateswara Rao P (2008) Experimental investigation of surface/subsurface damage formation and material removal mechanisms in sic grinding. Int J Mach Tools Manuf 48(6):698–710
13. Lambropoulos J (2000) From abrasive size to subsurface damage in grinding. In: Optical fabrication and testing. Optical Society of America, p OMA6
14. Jing X, Maiti S, Subhash G (2007) A new analytical model for estimation of scratch-induced damage in brittle solids. J Am Ceram Soc 90(3):885–892
15. Gu W, Yao Z, Li K (2011) Evaluation of subsurface crack depth during scratch test for optical glass bk7. Proc IME C J Mech Eng Sci 225(12):2767–2774
16. Chen J, Fang Q, Li P (2015) Effect of grinding wheel spindle vibration on surface roughness and subsurface damage in brittle material grinding. Int J Mach Tools Manuf 91:12–23
17. Li S, Wang Z, Wu Y (2008) Relationship between subsurface damage and surface roughness of optical materials in grinding and lapping processes. J Mater Process Technol 205(1):34–41
18. Wang C, Fang Q, Chen J, Liu Y, Jin T (2016) Subsurface damage in high-speed grinding of brittle materials considering kinematic characteristics of the grinding process. Int J Adv Manuf Technol 83:937–948
19. Quan J, Fang Q, Chen J, Xie C, Liu Y, Wen PH (2017) Investigation of subsurface damage considering the abrasive particle rotation in brittle material grinding. Int J Adv Manuf Technol 90:2461–2476
20. Malkin S, Guo C (2008) Grinding technology: theory and application of machining with abrasives. Industrial Press Inc
21. Song XF, Yin L (2010) The quantitative effect of diamond grit size on the subsurface damage induced in dental adjustment of porcelain surfaces. Proc Inst Mech Eng H J Eng Med 224(10):1185–1194
22. Axinte DA, Butlersmith PW, Akgun C, Kolluru K (2013) On the influence of single grit micro-geometry on grinding behavior of ductile and brittle materials. Int J Mach Tools Manuf 74:12–18
23. Malkin S, Hwang TW (1996) Grinding mechanisms for ceramics. CIRP Ann 45(2):569–580

24. Li S, Wang Z, Wu Y (2007) Relationship between subsurface damage and surface roughness of ground optical materials. J Cent South Univ Technol 14(4):546–551
25. Xu X, Li Y, Malkin S (2001) Forces and energy in circular sawing and grinding of granite. J Manuf Sci Eng Trans ASME 123(1):13–22
26. Pei ZJ, Billingsley SR, Miura S (1999) Grinding induced subsurface cracks in silicon wafers. Int J Mach Tools Manuf 39(7):1103–1116
27. Randi JA, Lambropoulos JC, Jacobs SD (2005) Subsurface damage in some single crystalline optical materials. Appl Opt 44(12):2241–2249
28. Lv D, Wang H, Zhang W, Yin Z (2016) Subsurface damage depth and distribution in rotary ultrasonic machining and conventional grinding of glass bk7. Int J Adv Manuf Technol 86:2361–2371
29. Ohta T, Yan J, Tsunemoto K, Kodera S, Nakasuji T (2007) Prediction of subsurface damage depth of ground brittle materials by surface profiling. Int J Mach Mach Mater 2(1):108–124
30. Liu C, Ding W, Yu T, Yang C (2018) Materials removal mechanism in high-speed grinding of particulate reinforced titanium matrix composites. Precis Eng 51:68–77
31. Qian N, Ding W, Zhu Y (2018) Comparative investigation on grindability of k4125 and inconel718 nickel-based superalloys. Int J Adv Manuf Technol 97(5–8):1649–1661
32. Dai C-W, Ding W-F, Zhu Y-J, Xu J-H, Yu H-W (2018) Grinding temperature and power consumption in high speed grinding of inconel 718 nickel-based superalloy with a vitrified cbn wheel. Precis Eng 52:192–200
33. Hu P, Zhang JM, Pei ZJ, Treadwell C (2002) Modeling of material removal rate in rotary ultrasonic machining: designed experiments. J Mater Process Technol 129(1):339–344
34. Schmitz TL, Ziegert JC (1999) Examination of surface location error due to phasing of cutter vibrations. Precis Eng-J Int Soc Precis Eng Nanotechnol 23(1):51–62
35. Ramesh K, Yeo SH, Gowri S, Zhou L (2001) Experimental evaluation of super high-speed grinding of advanced ceramics. Int J Adv Manuf Technol 17(2):87–92
36. Peng TV, Xu X (2013) A universal hybrid energy consumption model for cnc machining systems. In: Re-engineering manufacturing for sustainability. Springer, pp 251–256
37. Bastawros AF, Chandra A, Guo Y, Bo Y (2002) Pad effects on material-removal rate in chemical-mechanical planarization. J Electron Mater 31(10):1022–1031
38. Wang C, Chen J, Fang Q, Liu F, Liu Y (2016) Study on brittle material removal in the grinding process utilizing theoretical analysis and numerical simulation. Int J Adv Manuf Technol 87:2603–2614
39. Marinescu ID, Rowe B, Dimitrov B, Inasaki I (2004) Tribology of abrasive machining processes. J Manuf Sci Eng Trans ASME 126(4):859–859
40. Zhang X, Arif M, Liu K, Kumar AS, Rahman M (2013) A model to predict the critical undeformed chip thickness in vibration-assisted machining of brittle materials. Int J Mach Tools Manuf 69:57–66
41. Williams JA (1996) Analytical models of scratch hardness. Tribol Int 29(8):675–694